

Chiral Altermagnon in MnTe

Daniel Jost,^{1,2,*} Resham B. Regmi,^{3,4} Samuel Sahel-Schackis,^{1,2,5} Monika Scheufele,^{6,7} Marcel Neuhaus,² Rachel Nickel,⁸ Flora Yakhou,⁸ Kurt Kummer,⁸ Nicholas Brookes,⁸ Lingjia Shen,² Georgi L. Dakovski,² Nirmal J. Ghimire,^{3,4} Stephan Geprägs,⁶ and Matthias F. Kling^{1,2,9}

¹Stanford PULSE Institute, SLAC National Accelerator Laboratory, Menlo Park, CA, USA

²Linac Coherent Light Source, SLAC National Accelerator Laboratory, Menlo Park, CA, USA

³Department of Physics and Astronomy, University of Notre Dame, Notre Dame, IN 46556, USA

⁴Stravropoulos Center for Complex Quantum Matter,

University of Notre Dame, Notre Dame, IN 46556, USA

⁵Department of Physics, Stanford University, Stanford, CA, 94305, USA

⁶Walther-Meißner-Institut, Bayerische Akademie der Wissenschaften, 85748 Garching, Germany

⁷Technical University of Munich, TUM School of Natural Sciences, Physics Department, Garching, Germany

⁸European Synchrotron Radiation Facility, BP 220, F-38043, Grenoble Cedex, France

⁹Department of Applied Physics, Stanford University, Stanford, California 94305, USA

(Dated: January 30, 2025)

Altermagnetism has surfaced as a novel magnetic phase, bridging the properties of ferro- and anti-ferromagnetism. The momentum-dependent spin-splitting observed in these materials reflects their unique symmetry characteristics which also establish the conditions for chiral magnons to emerge. Here we provide the first direct experimental evidence for a chiral magnon in the altermagnetic candidate MnTe, revealed by circular-dichroism resonant inelastic X-ray scattering (CD-RIXS). This mode which we term chiral altermagnon exhibits a distinct momentum dependence consistent with the proposed altermagnetic g -wave symmetry of MnTe. Our results reveal a new class of magnetic excitations, demonstrating how altermagnetic order shapes spin dynamics and paves the way for advances in spintronic and quantum technologies.

I. INTRODUCTION

Chiral magnons - collective modes which exhibit a definite handedness - are an emerging frontier, offering exciting opportunities to enable spintronic devices and spin-based information processing.¹⁻⁷ Traditionally, such excitations have been associated with magnets exhibiting either net magnetization or complex spin textures.^{8,9} However, recent theoretical advances suggest that chiral magnons^{10,11} may also arise in so called altermagnets¹²⁻¹⁴ which have a net-zero magnetization.

A proposed altermagnet, manganese telluride (MnTe)¹⁸ represents an ideal platform to explore this notion. While hosting robust A -type anti-ferromagnetic order [Figure 1(a)],¹⁵⁻¹⁷ it displays electronic and magnetic properties¹⁹⁻²⁴ unexpected for an anti-ferromagnet.^{25,26} More fundamentally, its crystalline structure breaks inversion and translation symmetry which are key ingredients for altermagnetism.^{13,14} As a consequence, anisotropies imprint on the spin structure and shape the symmetry of the altermagnetic order parameter in MnTe, characterized by a predicted g -wave-like spin polarization [Figure 1(b)].¹³ This g -wave symmetry captures the effect of broken inversion and translational symmetries, thereby enforcing a momentum-dependent splitting of the electronic band structure, recently confirmed in photo-emission experiments.¹⁹⁻²² Similarly, collective magnetic excitations (i.e. magnons) which would nominally remain degenerate in anti-ferromagnets are expected to split in certain momentum-space regions.²⁷ Initial observations

suggest that such a splitting indeed occurs.²³ Taken together, these results provide strong evidence that MnTe realizes altermagnetism and presents a compelling arena to reveal the chiral magnetic excitations foreseen to emerge in altermagnets.¹⁴

In real space, these magnons can be visualized as spin rotations which precess out of phase with neighbors in adjacent sublattice planes, preserving net-zero magnetization [Figure 1(c), see Movie S1 for details]. As the degeneracy of the magnetic branches is lifted, the sublattice excitations are decoupled and the spin polarization expresses a spatial dependence. In a momentum-space perspective, as schematically shown in Figure 1(d), the spin polarization varies across the Brillouin zone (BZ), consistent with g -wave symmetry. These symmetry constraints enforce nodal lines and promote chiral magnetic excitations in distinct sectors of the BZ.

II. METHODS

A. Sample synthesis

Single crystals of MnTe were grown by the Tin-flux method. Mn pieces (Thermo scientific; 99.9%), Te shots (Thermo scientific; 99.999%), and Sn shots (Thermo scientific; 99.9999%) were loaded in a 5-ml aluminum oxide crucible in a molar ratio of 1:1:20. The crucible was sealed in a fused silica ampule under vacuum and heated to 960°C over 10 h, homogenized at 960°C for 12 h, and then cooled to 840°C over 100 h. After reach-

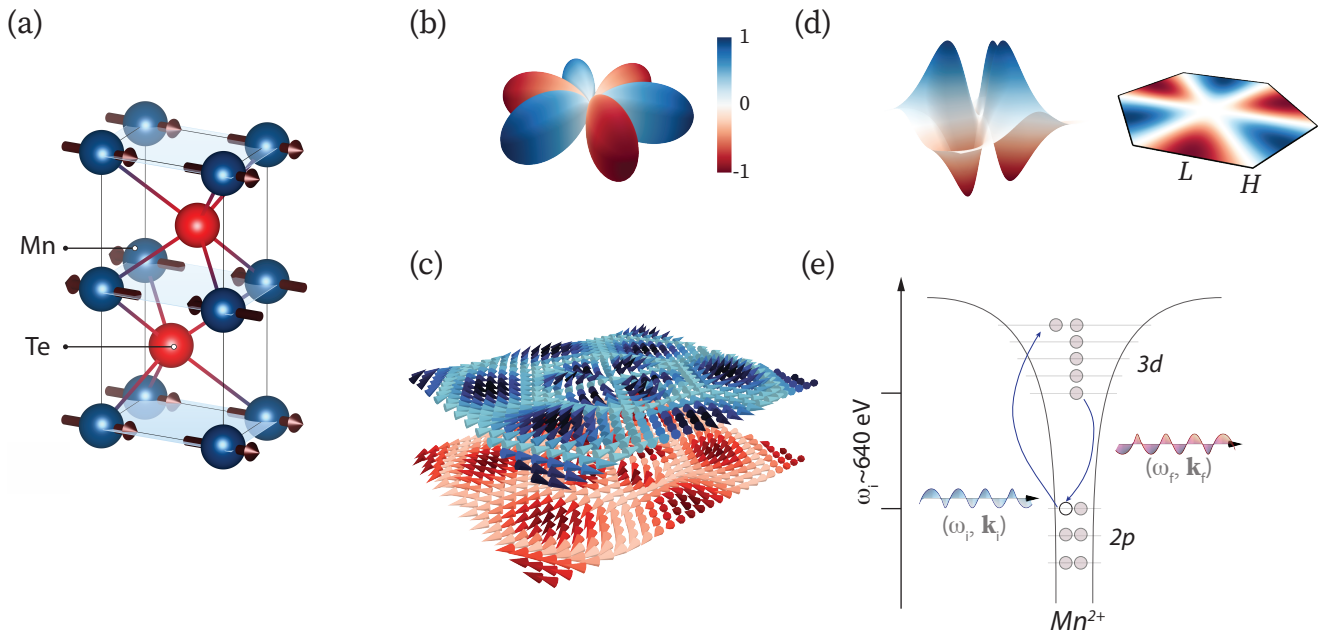


FIG. 1. **Crystalline structure, alternemagnetic spin polarization as well as collective magnetic excitations probed by resonant inelastic X-ray scattering (RIXS).** (a) Primitive unit cell of MnTe showing the ferromagnetic spin ordering within each plane separated by non-magnetic Te atoms, and their anti-ferromagnetic stacking.^{15–17} Along with the magnetically inert Te spacer layers, the crystal structure breaks inversion and translation symmetry which are key ingredients for alternemagnetism.^{13,14} (b) Alternemagnetic g -wave symmetry of the order parameter predicted for MnTe. The color gradient represents the spin polarization. (c) Collective magnetic excitations in real space represented as rotations of the spins sitting on each site of the hexagonal lattice. (d) Reciprocal space representation of the spin polarization. The right-hand image represents a projection onto the first Brillouin zone. (e) Schematic of the CD-RIXS process for a transition from Mn $2p$ core level to $3d$ orbitals which harbor an $S = 5/2$ spin configuration and subsequent de-excitation, filling the core hole upon emitting a photon of energy $\omega = \omega_i - \omega_f$ and momentum $\mathbf{q} = \mathbf{k}_i - \mathbf{k}_f$.

ing 840°C the excess flux was decanted from the crystals using a centrifuge leaving behind well-faceted shiny multiple hexagonal single crystals with few millimeters in dimensions.

B. X-ray scattering

X-Ray Absorption Spectroscopy (XAS) and Resonant Inelastic X-ray Scattering (RIXS) measurements were performed at the ID32 beamline of the European Synchrotron Research Facility (ESRF) using left- and right-handed circularly polarized light.²⁸ The combined energy resolution (beamline and spectrometer) was ~ 21 meV at the Mn L_3 edge (640 eV). As described in the text, the incident photon energy was tuned to optimize the feature in the inelastic spectrum at $\omega \sim 35$ meV. Both the sample (using the four-circle high-precision goniometer) and the scattering arm were moved to measure different points in momentum space. The momentum dependent measurements were conducted at $(0.1, 0.1, 0.5)$ r.l.u. and along the $(0.2, 0, \ell)$ r.l.u. and $(h, 0, 0.5)$ r.l.u. directions with units given in reciprocal lattice units (r.l.u.) of the hexagonal unit cell, having lattice parameters $a = b = 4.17$ Å and $c = 6.75$ Å. The sample

temperature was set to 30 K.

III. RESULTS

To capture chiral excitations experimentally, circular dichroism resonant inelastic X-ray scattering (CD-RIXS) has developed into a promising tool.^{29,30} In this work, circularly polarized photons were used to excite electrons from the Mn $2p$ core levels to its half-filled $3d$ orbitals [Figure 1(e)]. Within the lifetime of this intermediate state, energy transferred from the incident photons can create magnetic excitations which manifest as red-shifted, i.e. inelastic, features upon spectrally resolving the scattered photon energy.³¹ To locate a clean resonance condition of the magnetic excitation, we tuned the incident photon energy ω_i across the Mn L_3 absorption edge. Indeed, such an incident photon energy dependence revealed a feature in the inelastic spectrum appearing just below the fluorescence main peak energy [Figure 2(a)]. This excitation is located at an energy transfer of $\omega \sim 35$ meV [Figure 2(b)], an energy scale that aligns with the previously reported magnon band in MnTe.^{23,32}

To further corroborate the magnetic origin, we mea-

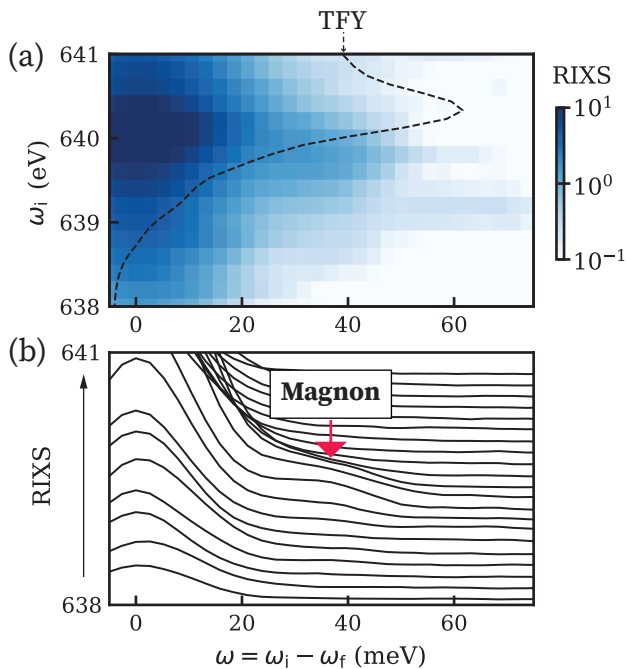


FIG. 2. **Magnetic excitations of MnTe as seen in RIXS.** (a) Incident photon energy ω_i dependence of the RIXS signal across the Mn L_3 edge. The total fluorescence yield (TFY) is shown as dashed line. (b) Stacked plot highlighting how the magnon shoulder develops slightly off-tuned from the maximum fluorescence signal of the Mn L_3 edge, approximately at $\omega \sim 35$ meV. The data was taken at $q = (0.03, 0, 0.5)$ r.l.u.

sured its momentum dependence along a trajectory in the Brillouin zone (BZ) [Figure 3(a)]. In hexagonal anti-ferromagnets with anti-parallel spins aligned along the c -axis, the magnon dispersion typically exhibits its maximum bandwidth at $(0,0,0.5)$ reciprocal lattice units (r.l.u.) at the A -point [Figure 3(b)], as is the case for MnTe.^{23,32} Conversely, the magnon mode disperses to zero as it approaches the Γ point [Figure 3(b)], reflecting the broken spin-rotational symmetry.³³ This behavior also holds for MnTe where the magnon shifts away from the elastic line as the out-of-plane momentum component is tuned towards the $A-L$ plane [see Figure 3(c) and figure S1].

Having confirmed its magnetic origin, we focused on probing its chirality. The spin polarization in momentum space representation [Figure 1 (d)] indicates a significant anisotropy in chiral magnon intensity. In this picture, a lifted degeneracy manifests as a dichroic signal in a region of the BZ exhibiting a non-zero spin polarization. Conversely, along nodal directions, the dichroism is expected to vanish, as the spin polarization is suppressed.

Towards the $A-L$ direction at $(0.2, 0, 0.5)$ r.l.u., a pronounced difference of the magnon intensity is seen for the two polarization channels, as depicted in Figure 4(a). This difference in intensity reflects the orbital angular momentum transfer associated with the excitation, providing a direct measure of the magnon chirality. In other

words, as altermagnets exhibit a momentum-dependent spin-polarization,¹⁴ the sub-lattice decoupling manifests as selective sensitivity to one circular polarization, a hallmark of their fundamentally broken inversion and translational symmetry.

Subtracting these two spectra yields a peak-like signature that encapsulates the chiral portion of the magnetic excitations. We term this excitation a chiral altermagnon (CAM). Modulating the momentum transfer from $(0.2, 0, 0.5)$ r.l.u. towards the A -point decreases the CAM intensity systematically [Figure 4(b),(c)], consistent with the picture drawn in Figure 1(d). This intensity dispersion, along with a vanishingly small circular dichroism along the nodal direction [see figure S2] is consistent with an altermagnetic spin polarization.

IV. DISCUSSION AND CONCLUSION

We note that along the $A-L$ direction, an energy splitting was not observed in a prior neutron scattering study.²³ However, in this work, the CAM width obtained from CD-RIXS differs between the two polarization channels [Figure 4(d)], indicating distinct lower bounds for the magnon lifetimes. The subdominant branch exhibits a broader peak (shorter lifetime), whereas the width of the dominant branch remains essentially constant and is near the instrumental resolution limit. These observations could imply that any lifting of degeneracy is governed more by damping than by a resolvable energy gap. Consequently, a conventional inelastic neutron scattering probe might not detect a splitting precisely where CD-RIXS reveals strong dichroism. However, future experiments at higher resolution - both RIXS and polarized inelastic neutron scattering - will be essential to resolve this apparent discrepancy. With these, it may be possible to clarify whether a small energy splitting or purely lifetime-based effects (or both) underlie the observed CAM response.

We have demonstrated that chiral altermagnons arise in MnTe, an anti-ferromagnet that displays characteristics canonically associated with finite magnetization. The pronounced dichroic signal whose momentum-dependence aligns with the altermagnetic g -wave symmetry underscores how broken spatial symmetries may foster chirality in otherwise collinear spin systems. Moreover, our results complete a crucial triad in the rapidly developing field of altermagnetism: the observations of spin-split electronic band structures,¹⁹⁻²² the splitting of magnon bands,²³ and now, the direct experimental observation of chirality in magnetic excitations, which positions MnTe as the archetypal altermagnet.

Future investigations will need to address the role of chiral magnons in shaping both transport and spectroscopic properties of altermagnetic materials. Advancing this field further will require a robust theoretical framework that captures the momentum-resolved nature of these excitations and their interaction with electronic and

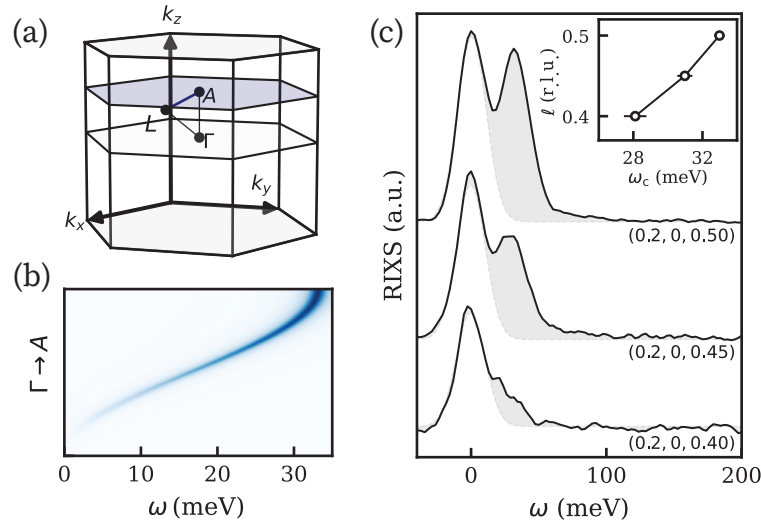


FIG. 3. **Magnetic dispersion along k_z .** (a) Hexagonal Brillouin zone of MnTe, with the triangle spanned by the points Γ , A and L indicating the region of interest in this work. (b) Illustration of a magnon dispersion for the $\Gamma \rightarrow A$ direction from a generic Heisenberg model. (c) RIXS spectra at indicated momentum points showing the shoulder at $(0.2, 0, 0.4)$ r.l.u. developing into a sharp peak for larger momentum. The in-plane momentum was off-tuned along h from specular reflection to reduce the elastic line intensity [see figure S1]. The inset shows the peak positions ω_c of the magnetic excitation.

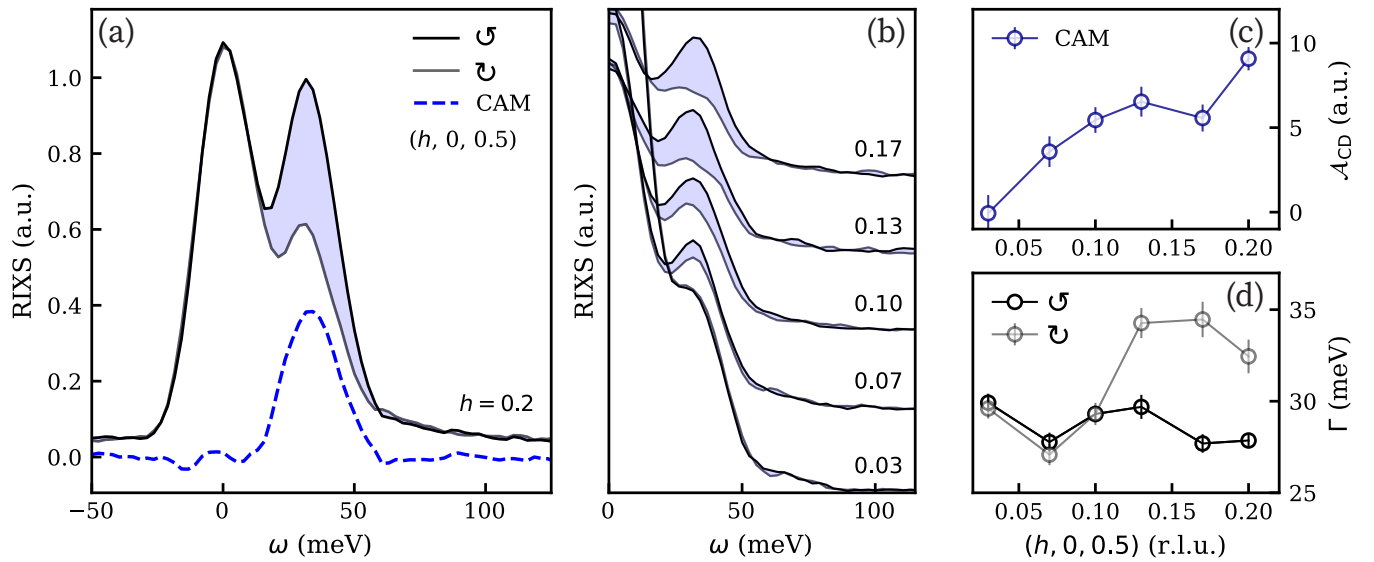


FIG. 4. **Evidence of chiral altermagnons.** (a) Spectra of the magnetic excitations for the two orthogonal circular polarization channels at the indicated point in the BZ. The subtraction of the signals in the two channels demonstrates the chiral nature of magnons in MnTe. (b) Momentum dependence of the chiral altermagnon (CAM) which vanishes towards the high-symmetry A -point. At high-symmetry points, the modes with opposite chirality are degenerate leading to equal RIXS intensities using circularly polarized light. (c) Intensity dispersion of the CAM where $\mathcal{A}_{CD} = \mathcal{A}_{\odot} - \mathcal{A}_{\ominus}$ which increases systematically towards the center of the $A - L$ direction. (d) Width of the magnetic excitation in the two orthogonal polarization channels which shows a significant broadening for the subdominant magnon branch suggesting a lifetime decrease.

magnetic degrees of freedom, including damping-driven effects.

Lastly, as altermagnets lack stray magnetic fields, they are ideal for compact and interference-free device integration. By demonstrating that altermagnets host chiral excitations, our work paves the way for novel spin-based ap-

plications in which chiral altermagnons take center stage.

Author contributions D.J. conceived the study, led the experiment and analyzed the data. D.J., S.S.S., M.S., M.N., R.N. and S.G. performed the experiments. R.B.R. and N.J.G. synthesized and characterized the samples. D.J. wrote the first draft. D.J., R.B.R., S.S.S., M.S.,

M.N., R.N., F.Y., K.K., N.B., L.S., G.L.D., N.J.G., S.G., and M.F.K. discussed and interpreted the results and contributed to the final version of the manuscript.

ACKNOWLEDGMENTS

This work was supported by the Department of Energy, Basic Energy Science. The experiment was per-

formed at the European Synchrotron Radiation Facility in Grenoble, France under proposal HC-5866, DOI: 10.15151/ESRF-ES-1901557821.

-
- * daniel.jost@stanford.edu
- ¹ L. Šmejkal, Y. Mokrousov, B. Yan, and A. H. MacDonald, *Nature Physics* **14**, 242 (2018).
 - ² Y. Tokura, K. Yasuda, and A. Tsukazaki, *Nature Reviews Physics* **1**, 126 (2019).
 - ³ G. Dieterle, J. Förster, H. Stoll, A. S. Semisalova, S. Finizio, A. Gangwar, M. Weigand, M. Noske, M. Fähnle, I. Bykova, J. Gräfe, D. A. Bozhko, H. Y. Musienko-Shmarova, V. Tiberkevich, A. N. Slavin, C. H. Back, J. Raabe, G. Schütz, and S. Wintz, *Phys. Rev. Lett.* **122**, 117202 (2019).
 - ⁴ T. Yu, Y. M. Blanter, and G. E. W. Bauer, *Phys. Rev. Lett.* **123**, 247202 (2019).
 - ⁵ H. Wang, J. Chen, T. Liu, J. Zhang, K. Baumgaertl, C. Guo, Y. Li, C. Liu, P. Che, S. Tu, S. Liu, P. Gao, X. Han, D. Yu, M. Wu, D. Grundler, and H. Yu, *Phys. Rev. Lett.* **124**, 027203 (2020).
 - ⁶ S.-H. Yang, *Applied Physics Letters* **116**, 120502 (2020).
 - ⁷ S.-H. Yang, R. Naaman, Y. Paltiel, and S. S. P. Parkin, *Nature Reviews Physics* **3**, 328 (2021).
 - ⁸ A. Fert, N. Reyren, and V. Cros, *Nature Reviews Materials* **2**, 17031 (2017).
 - ⁹ Y. Zhou, S. Li, X. Liang, and Y. Zhou, *Advanced Materials* **n/a**, 2312935 (2024).
 - ¹⁰ Y. Nambu, J. Barker, Y. Okino, T. Kikkawa, Y. Shiomi, M. Enderle, T. Weber, B. Winn, M. Graves-Brook, J. M. Tranquada, T. Ziman, M. Fujita, G. E. W. Bauer, E. Saitoh, and K. Kakurai, *Phys. Rev. Lett.* **125**, 027201 (2020).
 - ¹¹ S.-W. Cheong and X. Xu, *npj Quantum Materials* **7**, 40 (2022).
 - ¹² L. Šmejkal, R. González-Hernández, T. Jungwirth, and J. Sinova, *Science Advances* **6**, eaaz8809 (2020).
 - ¹³ L. Šmejkal, J. Sinova, and T. Jungwirth, *Physical Review X* **12** (2022).
 - ¹⁴ L. Šmejkal, J. Sinova, and T. Jungwirth, *Physical Review X* **12** (2022).
 - ¹⁵ Kunitomi, Nobuhiko, Hamaguchi, Yoshikazu, and Anzai, Shuichiro, *J. Phys. France* **25**, 568 (1964).
 - ¹⁶ J. Efrem D'Sa, P. Bhohe, K. Priolkar, A. Das, S. Paranjpe, R. Prabhu, and P. Sarode, *Journal of Magnetism and Magnetic Materials* **285**, 267 (2005).
 - ¹⁷ D. Kriegner, H. Reichlova, J. Grenzer, W. Schmidt, E. Ressouche, J. Godinho, T. Wagner, S. Y. Martin, A. B. Shick, V. V. Volobuev, G. Springholz, V. Holý, J. Wunderlich, T. Jungwirth, and K. Výborný, *Physical Review B* **96** (2017).
 - ¹⁸ R. Juza, A. Rabenau, and G. Pascher, *Zeitschrift für anorganische und allgemeine Chemie* **285**, 61 (1956).
 - ¹⁹ J. Krempaský, L. Šmejkal, S. W. D'Souza, M. Hajlaoui, G. Springholz, K. Uhlířová, F. Alarab, P. C. Constantinou, V. Strocov, D. Usanov, W. R. Pudelko, R. González-Hernández, A. Birk Hellenes, Z. Jansa, H. Reichlová, Z. Šobáň, R. D. Gonzalez Betancourt, P. Wadley, J. Sinova, D. Kriegner, J. Minár, J. H. Dil, and T. Jungwirth, *Nature* **626**, 517 (2024).
 - ²⁰ S. Lee, S. Lee, S. Jung, J. Jung, D. Kim, Y. Lee, B. Seok, J. Kim, B. G. Park, L. Šmejkal, C. J. Kang, and C. Kim, *Physical Review Letters* **132** (2024).
 - ²¹ T. Osumi, S. Souma, T. Aoyama, K. Yamauchi, A. Honma, K. Nakayama, T. Takahashi, K. Ohgushi, and T. Sato, *Physical Review B* **109** (2024).
 - ²² M. Hajlaoui, S. Wilfred D'Souza, L. Šmejkal, D. Kriegner, G. Krizman, T. Zakusylo, N. Olszowska, O. Caha, J. Michalička, J. Sánchez-Barriga, A. Marmodoro, K. Výborný, A. Ernst, M. Cinchetti, J. Minar, T. Jungwirth, and G. Springholz, *Advanced Materials* **36**, 2314076 (2024).
 - ²³ Z. Liu, M. Ozeki, S. Asai, S. Itoh, and T. Masuda, *Phys. Rev. Lett.* **133**, 156702 (2024).
 - ²⁴ O. J. Amin, A. Dal Din, E. Golias, Y. Niu, A. Zakharov, S. C. Fromage, C. J. B. Fields, S. L. Heywood, R. B. Cousins, F. Maccherozzi, J. Krempaský, J. H. Dil, D. Kriegner, B. Kiraly, R. P. Champion, A. W. Rushforth, K. W. Edmonds, S. S. Dhesi, L. Šmejkal, T. Jungwirth, and P. Wadley, *Nature* **636**, 348 (2024).
 - ²⁵ N. Nagaosa, J. Sinova, S. Onoda, A. H. MacDonald, and N. P. Ong, *Rev. Mod. Phys.* **82**, 1539 (2010).
 - ²⁶ L. Šmejkal, A. H. MacDonald, J. Sinova, S. Nakatsuji, and T. Jungwirth, *Nature Reviews Materials* **7**, 482 (2022).
 - ²⁷ L. Šmejkal, A. Marmodoro, K.-H. Ahn, R. González-Hernández, I. Turek, S. Mankovsky, H. Ebert, S. W. D'Souza, O. c. v. Šipr, J. Sinova, and T. c. v. Jungwirth, *Phys. Rev. Lett.* **131**, 256703 (2023).
 - ²⁸ N. Brookes, F. Yakhou-Harris, K. Kummer, A. Fondacaro, J. Cezar, D. Betto, E. Velez-Fort, A. Amorese, G. Ghiringhelli, L. Braicovich, *et al.*, *Nuclear Instruments and Methods in Physics Research Section A: Accelerators, Spectrometers, Detectors and Associated Equipment* **903**, 175 (2018).
 - ²⁹ M. Schüler, T. Schmitt, and P. Werner, *npj Quantum Materials* **8**, 6 (2023).
 - ³⁰ H. Ueda, M. García-Fernández, S. Agrestini, C. P. Romao, J. van den Brink, N. A. Spaldin, K.-J. Zhou, and U. Staub, *Nature* **618**, 946 (2023).
 - ³¹ L. J. P. Ament, M. van Veenendaal, T. P. Devereaux, J. P. Hill, and J. van den Brink, *Rev. Mod. Phys.* **83**, 705 (2011).

- ³² W. Szuszkiewicz, B. Hennion, B. Witkowska, E. Łusakowska, and A. Mycielski, *Physica Status Solidi C: Conferences* **2**, 1141 (2005).
- ³³ J. Goldstone, A. Salam, and S. Weinberg, *Phys. Rev.* **127**, 965 (1962).

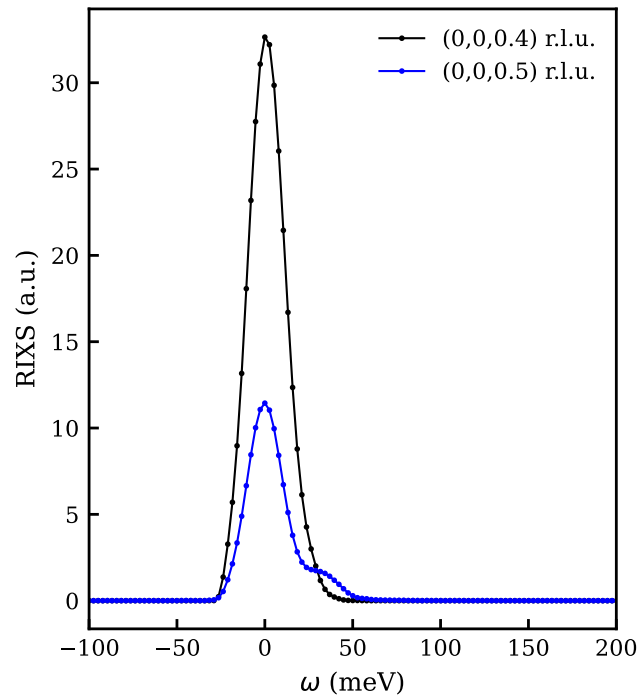


FIG. S1. **Momentum dependence along the $\Gamma - A$ -direction.** RIXS measurement at (0, 0, 0.4) r.l.u. and (0,0,0.5) r.l.u. showing the magnetic excitation off the elastic line at the A -point. The strong elastic contribution is due to specular reflection.

SUPPLEMENTARY MATERIAL

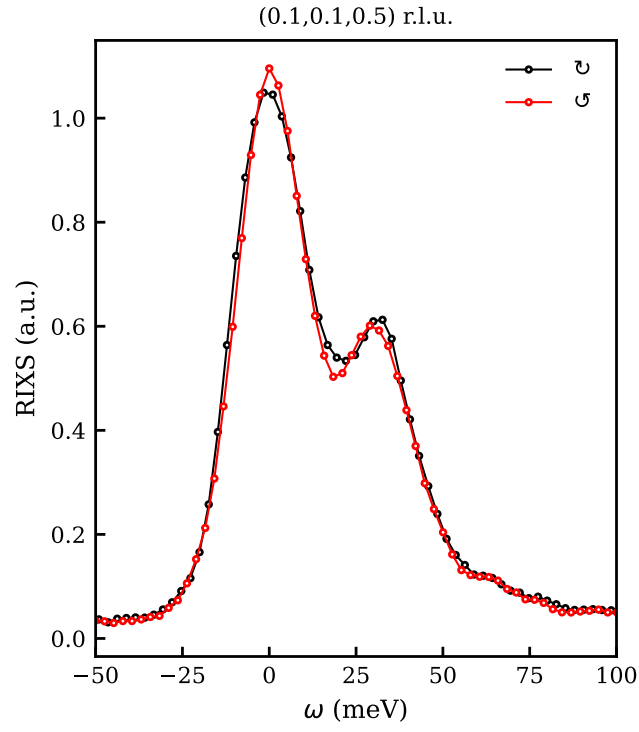


FIG. S2. **Circular dichroism measurement along the nodal direction.** CD-RIXS measurement at (0.1, 0.1, 0.5) r.l.u. showing a strongly suppressed dichroism compared to an equivalent momentum point along the $A - L$ -direction.